PCCP

Accepted Manuscript

This is an *Accepted Manuscript*, which has been through the Royal Society of Chemistry peer review process and has been accepted for publication.

Accepted Manuscripts are published online shortly after acceptance, before technical editing, formatting and proof reading. Using this free service, authors can make their results available to the community, in citable form, before we publish the edited article. We will replace this *Accepted Manuscript* with the edited and formatted *Advance Article* as soon as it is available.

You can find more information about *Accepted Manuscripts* in the Information for Authors.

Please note that technical editing may introduce minor changes to the text and/or graphics, which may alter content. The journal's standard Terms & Conditions and the Ethical guidelines still apply. In no event shall the Royal Society of Chemistry be held responsible for any errors or omissions in this *Accepted Manuscript* or any consequences arising from the use of any information it contains.

ROYAL SOCIETY OF CHEMISTRY

www.rsc.org/pccp

Journal Name

ARTICLE

Variable Electronic Properties of Lateral Phosphorene-Graphene Heterostructures †

Received 00th January 20xx,

www.rsc.org/

Xiaoqing Tian,[a] Lin Liu,[a] Yu Du, *[a] Juan Gu, [a] Jian-bin Xu,*[b] and Boris I. Yakobson*[c]

Phosphorene and graphene have a tiny lattice mismatch along the armchair direction, which can result in an atomically sharp in-plane interface. The electronic properties of the lateral heterostructures of phosphorene/graphene are investigated by the first-principles method. Here, we demonstrate that the electronic properties of this type of heterostructure can be highly tunable by the quantum size effects and the externally applied electric field (E_{ext}). At strong E_{ext} , Dirac Fermions can be deveoped with Fermi velocities around one order smaller than that of graphene. Undoped and hydrogen doped configurations demonstrate three drastically different electronic phases, which reveal the strongly tunable potential of this type of heterostructure. Graphene is a naturally better electrode for phosphorene. The transport properties of two-probe devices of graphene/phosphorene/graphene exhibit tunnelling transport characteristics. Given these results, it is expected that in-plane heterostructures of phosphorene/graphene will present abundant opportunities for applications in optoelectronic and electronic devices.

1. Introduction

As a new form of two-dimensional material in the 'post-graphene age', black phosphorous has attracted intense research interest since its potential application in field-effect transistors was first demonstrated.[1-3] Layered black phosphorus (phosphorene) has a buckled honeycomb structure and adjacent phosphorene layers are coupled by weak van der Waals interactions. Different from white and red phosphorus, phosphorene is less reactive and is thermodynamically stable below 550°C. As a mono-elemental semiconductor, monolayer phosphorene has an intrinsic band gap of 2 eV. This exceeds that of graphene, which needs an externally applied electric field or doping to open a band gap.[4-9] The intrinsic anisotropic electronic and thermal transport properties of phosphorene have been theoretically predicted.[10-12] The electronic and optoelectronic properties can be modulated by the strain, and atomic and molecular doping.[13-19] Moreover, unlike semiconducting MoS_2, which may naturally contain defects,[20] phosphorene is a monoelemental semiconductor, which makes the structure simpler and results in a lower defect concentration. Analogous to oxide heterostructures, the in-plane interfaces between graphene and hexagonal boron nitride possess unusual electronic, magnetic and optical properties.[21,22] Recently, in-plane heterostructures of phosphorene and a variety of carbon materials including graphite, graphite oxide, carbon black and fullerene have been fabricated in experiments.[23] Although these heterostructures are demonstrated to be stable and high capacity anode materials, the geometrical and electronic structures have not been revealed. Here, we use the state-of-art first principles method to study the electronic properties of the in-plane heterostructures of phosphorene and graphene.

2. Computational methods

The first-principle calculations were performed with the Quantum espresso package.[24] The electron-ion interaction was described by the projector augmented wave (PAW) method.[25] The plane-wave basis set cut-off energy was 400 eV. The Perdew-Burke-Ernzerh (PBE) type of generalised gradient approximation exchange correlation function was used.[6] Long-range van der Waals dispersion corrections according to the DFT-D procedure were taken into account.[27] Quantum transport properties were performed with the nanodcal package.[28] The energy convergence criterion for the electronic wave function was set to be 10^{-5} eV. The geometry optimization was considered to be converged when the

Physical Chemistry Chemical Physics Accepted Manuscript

This journal is © The Royal Society of Chemistry 20xx

residual force on each atom was smaller than 0.01 eV/Å. A 2.5 nm thick vacuum layer normal to the plane was used to eliminate longitudinal interactions between the super cells. The 1.6 nm vacuum layer was used to laterally separate the one dimensional (1-D) heterostructures. Sampling of 30 uniformly distributed k-points along the 1-D Brillouin zone was used for the calculations.

3. Results and discussion

3.1 Electronic structures of heterostructures

Phosphorene and graphene have a slight lattice mismatch of 2.6 per cent along the armchair direction, which can result in an atomically sharp interface. A variety of heterostructures of armchair phosphorene nanoribbons (APNRs) and armchair graphene nanoribbons (AGNRs) are considered. The width (N) of the APNRs and AGNRs is defined by the number of atomic columns along the zigzag direction as shown in Fig. 1(a). A typical heterostructure of 15-APNR/15-AGNR is demonstrated here, and the relaxed structure is shown in Figs. 1(a) and 1(b). Its width is 4.4 nm. At the central region of this heterostructure, 15-APNR interfaces 15-AGNR, which are connected by robust chemical bonds. The length of the P-C bond is 1.86 Å at this interface, which is within the interval of C-C (1.42 Å) and P-P (2.17 Å) bonds.

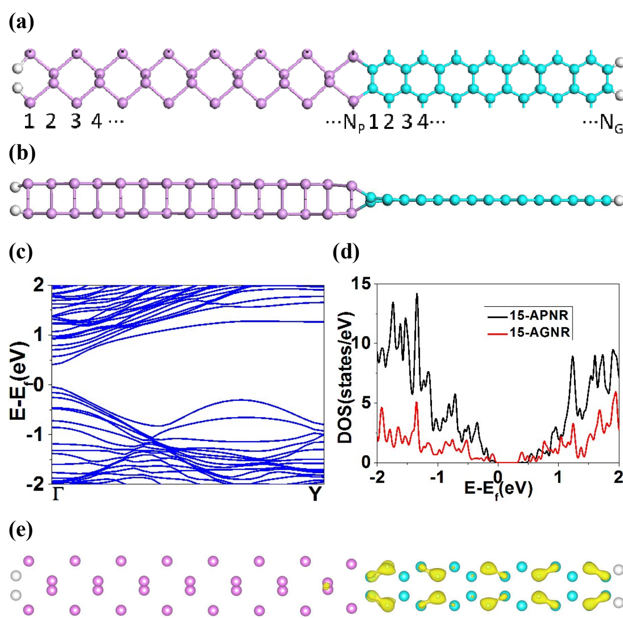

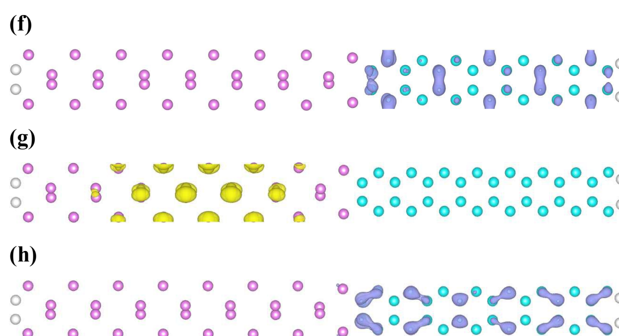

Fig. 1 (a) Top and (b) side views of the relaxed heterostructure of 15-APNR/15-AGNR. (c) Band structure and (d) DOS of 15-APNR/15-AGNR. Charge distributions of (e) HOMO and (f) LUMO of 15-APNR/15-AGNR. Charge distributions of (g) HOMO and (h) LUMO of 15-APNR/16-AGNR. The white, pink and cyan circles denote H, P and C atoms, respectively.

The heterostructure of 15-APNR/15-AGNR has a direct band gap of 0.45 eV at Γ as shown in Fig. 1(c). Its corresponding density of states (DOS) is shown in Fig. 1(d). Based on the DOS, the states of both the valence band maximum (VBM) and conduction band minimum (CBM) are mainly contributed from the orbitals of 15-AGNR. This is confirmed by the charge distribution of the HOMO and LUMO orbitals as shown in Figs. 1(e) and 1(f), respectively. The effective masses of the hole and electron carriers (m_h^* and m_e^*) are both 0.18 times that of a free electron (m_0) calculated by the parabolic dispersion

$$E_n(k) = E_{n0} + \frac{(\hbar k)^2}{2m^*} \qquad (1)$$

where k is the wave vector and E_{n0} is the band bottom of the nth subband. The m_h^* and m_e^* are at the VBM and CBM, respectively. According to the Drude model, electron and hole carriers have the same mobility. Because the states near Fermi level are mainly contributed from the 15-AGNR, the current will mainly flow through the right part of this heterostructure. The charge transfer at this interface is analysed using the Bader method. The valence states of the P and C atoms which form the P-C bonds are -1.2 and +1.2, respectively. The 15-AGNR attains 2.4 e in total from the 15-APNR per supercell. To understand the physical properties related to the field emission, chemical affinity and ionization of this heterostructure, the work function is calculated by

$$\Phi_w = \phi_0 e - E_F \qquad (2)$$

Physical Chemistry Chemical Physics Accepted Manuscript

This journal is © The Royal Society of Chemistry 20xx

where ϕ_0 is the electrostatic potential of a vacuum level far from the surface and E_F is the energy of the Fermi level.[29] Here, the calculated Φ_w is 4.34 eV, which is smaller than that of pristine graphene's theoretical value of 4.48 eV and the experimental value of 4.60 eV.[30,31]

To study the influence of the width of AGNRs on the electronic properties of heterostructures, the interface of 15-APNR/16-AGNR is studied. The VBM and CBM are mainly contributed from the 15-APNR and 16-AGNR, respectively (see Figs. 1(g) and 1(h)). The calculated Φ_w and band gap are 4.47 eV and 0.66 eV, respectively (see the ESI†). For comparison, the electronic properties of two-dimensional periodic stripes of APNRs/AGNRs are also investigated. Two-dimensional periodic stripes of APNRs/AGNRs exhibit semiconducting properties and the corresponding band gap values are smaller than the corresponding values of one-dimensional APNRs/AGNRs due to the interactions between neighbouring supercells (see the ESI†). This is due to the strict confinement of electrons along the X direction being relieved.

3.2 Quantum size and electric field effects

The obvious discrepancies in the electronic properties of the heterostructures of 15-APNR/16-AGNR and 15-APNR/15-AGNR can be understood by comparing the differences between the electronic properties of APNRs and AGNRs. As shown in Fig. 2(a), the band gaps of 15-APNR, 15-AGNR and 16-AGNR are 0.72, 0.57 and 0.76 eV, respectively. The band gaps of both 15-APNR/15-AGNR and 15-APNR/16-AGNR are smaller than those of the isolated APNR and AGNR. The band gap value is determined by the differences in the on-site energies of two edges, and intra- and inter-edge hopping parameters from the view of tight-binding ladder models.[32] The hybridization of electronic states via σ bonds at this interface will influence these parameters.

As shown in Fig. 2(a), the band gaps of APNRs and AGNRs obey drastically different mathematical functions. The band gaps of APNRs scale approximately as $1/N^2$, which can be interpreted as the kinetic energy of a nonrelativistic particle is proportional to the square of its momentum.[33] The band gaps of AGNRs scale approximately as $1/N$, which can be attributed to the Dirac fermions exhibiting as the linear energy-momentum dispersion relationship. For GNRs, the mathematical relationship of band gap versus width follows the two hierarchic rules of $\Delta E_{3n-1}<\Delta E_{3n}<\Delta E_{3n+1}$ and $\Delta E_N<\Delta E_{N+3}$.[34] This oscillating characteristic has been transferred to the electronic properties of the heterostructures of APNRs/AGNRs. The band gaps of the heterostructures of 7, 10, 15-APNRs interfaced *N*-AGNRs are calculated with *N* increased from 1 to 20 as shown in Fig. 2(b). For the heterostructure of a specific APNR/*N*-AGNR, the band gaps oscillate as *N* increases, and the two hierarchic rules of $\Delta E_{3n-1}<\Delta E_{3n}<\Delta E_{3n+1}$ and $\Delta E_N<\Delta E_{N+3}$ are still fulfilled if the width *N* is larger than 2.

An external electric field (E_{ext}) was applied across the width of the heterostructures of APNRs/AGNRs. The breakdown electrical field limit of SiO_2 dielectric materials is 0.1 V/Å. Given the relative dielectric constant of (ε_r) 3.9 of SiO_2, the effective electric field of 0.39 V/ Å (relative to vacuum) can be realized in the experiments. Recently, an effective electric field (relative to vacuum) of 0.27 V/Å has been realized in the experiments.[35] The scanning tunnelling microscope (STM) tip can also realize strong electric field locally. The E_{ext} can effectively reduce the band gaps of the heterostructures of APNRs/AGNRs as shown in Fig. 2(c). This is in contrast to the situation of bilayer graphene, but it is similar to the situation of monolayer graphene. For monolayer graphene, the band gap value is equal to the difference between the on-site energies of the AB lattices of graphene.[36] For bilayer graphene, the band gap values depend on the electrostatic potential differences between the top and bottom graphene layers, and the stronger the vertical electric field, the larger the band gap.[37] Here, at zero bias, the band gaps are the largest for all of the heterostructures investigated. At a critical electric field (E_c), the band gaps of these heterostructures are zero. The tranverse E_{ext} causes the additional potential energy difference of the two edges *U*, which is defined as $U=eE_{ext}(d_P/\kappa_P+d_G/\kappa_G)$, where κ_P and κ_G are the dielectric constants for APNRs and AGNRs, respectively. d_P and d_G are the widths of APNRs and AGNRs, respectively. Thus, for the same E_{ext}, a larger width of APNR and AGNR will cause a larger *U*. Correspondingly, the E_c will decrease. Each heterostructure has a positive E_c and a negative E_c. The values of E_cs (-0.35 and 0.25 V/Å) are the same for 15-APNR/15-AGNR and 15-APNR/16-AGNR, which can be mainly attributed to the tiny difference in width (~2 per cent). The values of E_c are -0.4 and 0.425 V/Å for the 10-APNR/8-AGNR, which are obviously larger than those of 15-APNR/15-AGNR. If the E_{ext} is increased from 0 to the E_c, the band gaps can be effectively

Physical Chemistry Chemical Physics Accepted Manuscript

reduced. However, the m_h^* and m_e^* are rarely changed if the E_{ext} is smaller than E_c. An E_{ext} smaller than E_c can narrow the difference between the CBM and VBM, but will not change the parabolic shapes of the bands. If the E_{ext} is larger than the E_c, the conduction and valence bands are crossed. The band structure of the heterostructure of 15-APNR/15-AGNR with an E_{ext} of 0.30 V/Å is shown in Fig. 2(d). As shown in Figs. 2(e) and 2(f), an E_{ext} stronger than the negative or positive E_cs can turn APNRs/AGNRs into metallic materials. As the strength of E_{ext} is further increased, the band crossing point will be far from the Γ point. The band crossing point can also be tuned either above or below the Fermi level. Moreover, the topmost valence bands at biases of -0.45 and 0.35 V/Å exhibit linear dispersion near the band crossing point along the Γ→Y direction. The linear region is from the band crossing point to around 0.4 eV below. The Fermi velocities are 9.2 and 6.1×10^4 m/s, respectively, at -0.45 and 0.35 eV/Å. Thus, with a strong transverse electric field, Dirac Fermions can be developed, with Fermi velocities around one order smaller than that of pristine graphene (10^6 m/s).

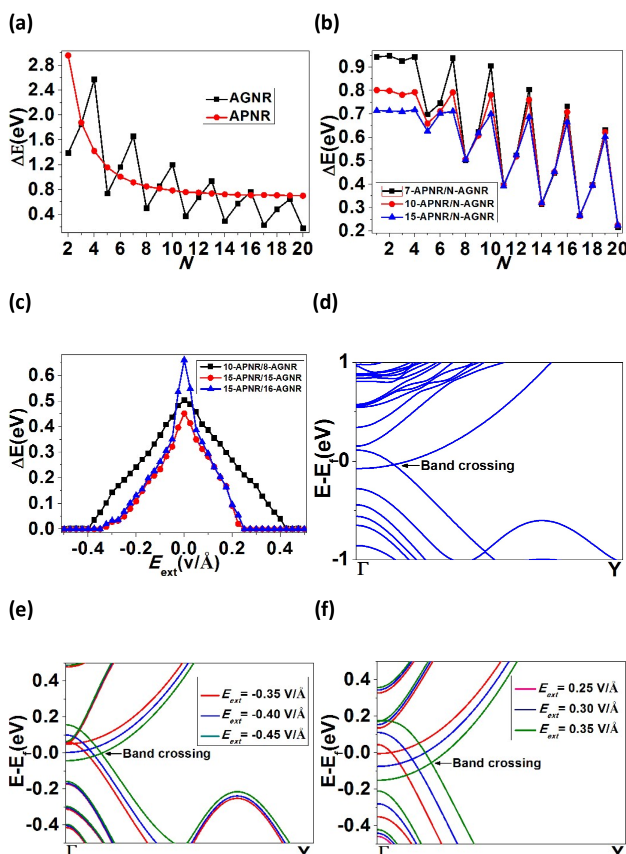

Fig. 2 (a) Band gaps of AGNRs and APNRs versus the width (N). (b) Band gaps of heterostructures of 7, 10 and 15-APNRs/ N-AGNRs versus the width of AGNRs. (c) Band gaps of heterostructures of APNRs/AGNRs versus the E_{ext}. (d) Band structure of 15-APNR/15-AGNR under an E_{ext} of 0.3 V/Å. Band structures of 15-APNR/15-AGNR with an E_{ext} of (e) negative and (f) positive values.

The band closure for these heterostructures can be explained by the tight-binding ladder model.[32] Suppose that the hopping integrals along the left and right edges are t_1 and t_2, respectively. The on-site energies of two edges are ε_l and ε_r, respectively. Then, the band structures of the two edges are $E_l(k)=\varepsilon_l-2t_1coska$ and $E_r(k)=\varepsilon_r-2t_2coska$. If the hopping integral between two edges is t_0, the Hamiltonian is as follows:

$$H=\begin{bmatrix} \varepsilon_l-\frac{U}{2}-2t_1coska & -t_0 \\ -t_0 & \varepsilon_r+\frac{U}{2}-2t_2coska \end{bmatrix} \quad (3)$$

Thus, the band structure near Fermi level takes the form

$$E(k)=\frac{E_l(k)+E_r(k)}{2}\pm\frac{1}{2}\sqrt{[E_l(k)-E_r(k)-U]^2+4t_0^{\,2}} \quad (4)$$

For Eq (3), the "+" symbol is for the conduction band and the "-" symbol is for the valence band. If there is no E_{ext} applied, U is zero. The band gap size will be $[(\varepsilon_l-\varepsilon_r)^2+4t_0^2]^{1/2}$ at Γ. When a transverse E_{ext} is applied, the minimum band gap size will be $2t_0$. If t_0 is reduced simultaneously as E_{ext} is increased, the electronic polarisation of the edge states under the E_{ext} reduces the effective interaction between the two edges of the heterostructure. If t_0 is zero, band gap closure occurs. Naturally, the wave vector of the band gap closure in k-space, k_{ext}, can be calculated from Eq (3). The wave vector of the band crossing point follows $k_{ext} = \{arccos\ [(U_0-U)/2(t_1-t_2)]\}/a$, with $U_0=\varepsilon_l-\varepsilon_r$. This qualitative picture can explain the monotonic variance of k_{ext} with E_{ext} as shown in Figs. 2(e) and 2(f). For more details of the tight-binding ladder model, see ESI.

3.3 Hydrogen doping effects

Experimental and theoretical studies have demonstrated that atomic H doping can strongly alter the physical properties of graphene.[38,39] Here, we study the influence of H doping on the electronic properties of the heterostructures of phosphorene/graphene. First, the adsorption of H monomer is investigated, and 30 adoption sites are considered (see ESI). The

Physical Chemistry Chemical Physics Accepted Manuscript

 This journal is © The Royal Society of Chemistry 20xx

two most stable configurations of H monomer doped 15-APNR/15-AGNR are shown in Figs. 3 (a) and 3(b), respectively. The adsorption energy is defined as

$$E_{ad} = -(E - E_0 - nE_H) / n \quad (5)$$

where E is the total energy of the heterostructure with H atoms adsorbed, E_H is the total energy of an isolated H atom, E_0 is the total energy of a heterostructure, and n is the number of H atoms.

The adsorption energies of configurations 1 and 2 are 1.84 and 1.80 eV, respectively. The highest adsorption energies indicate that the boundary between graphene and phosphorene is more chemically active. As shown in Fig. 3(c), for configuration 1, AGNR is strong strongly spin-polarised, whereas APNR is strong weakly spin-polarised. The total magnetisation is 1 Bohr magneton (μB), which is contributed from the unpaired 2*Pz* electron. Both the majority and minority spin bands have a band gap. For configuration 2, the Fermi level lies in the conduction bands of both APNR and AGNR (see Fig. 3(d)). The doping of H injects additional carriers into APNR and raises the Fermi level, which is even higher than the CBM. The total DOS of this heterostructure indicates the metallic signature.

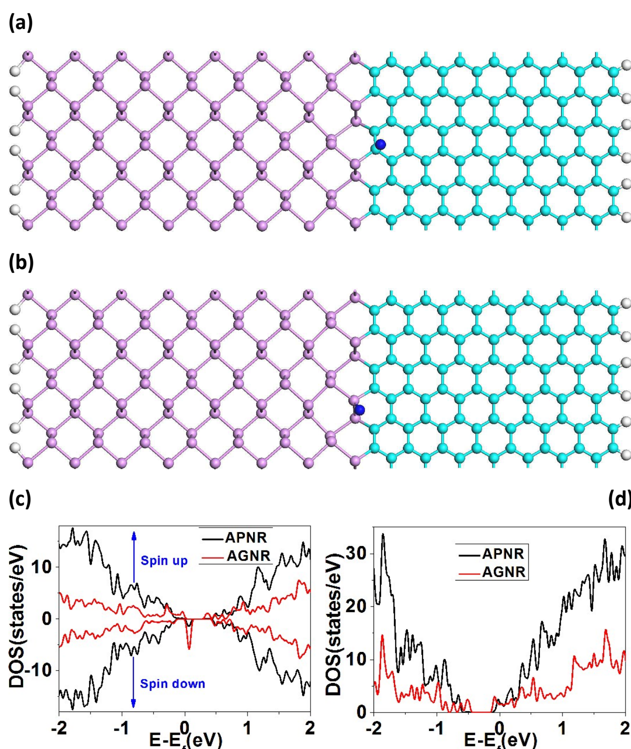

Fig. 3. Optimised structures of (a) configuration 1 and (b) configuration 2. DOS of (c) configuration 1 and (d) configuration 2. H adatoms are blue.

The concentration of H impurities is further increased. The adsorption of H dimmer on the heterostructure is investigated. For configuration 1, the H dimmer is adsorbed on both the top and bottom planes of the heterostructure as shown in Fig. 4(a). For configuration 1, the H dimmer is adsorbed on the left APNR side as shown in Fig. 4(b). These two different configurations result in two drastically different electronic properties. As shown in Fig. 4(c), configuration 1 exhibits as a semiconductor with a band gap of 0.32 eV, which is 0.13 eV smaller than that of the undoped 15-APNR/15-AGNR heterostructure. The doping of H dimmer affects the band gap states, which results in the band gap reduction. For configuration 2, the H doping injects excessive electron carriers into APNR and raises the Fermi level. The Fermi level is 0.22 eV above the CBM, so the heterostructure is heavily doped and exhibits metallic characteristics. Thus, the H doping effects can be concentration- and configuration-dependent. Moreover, H doping can cause magnetization, reduce the band gap and lead to semiconductor-to-metal transition.

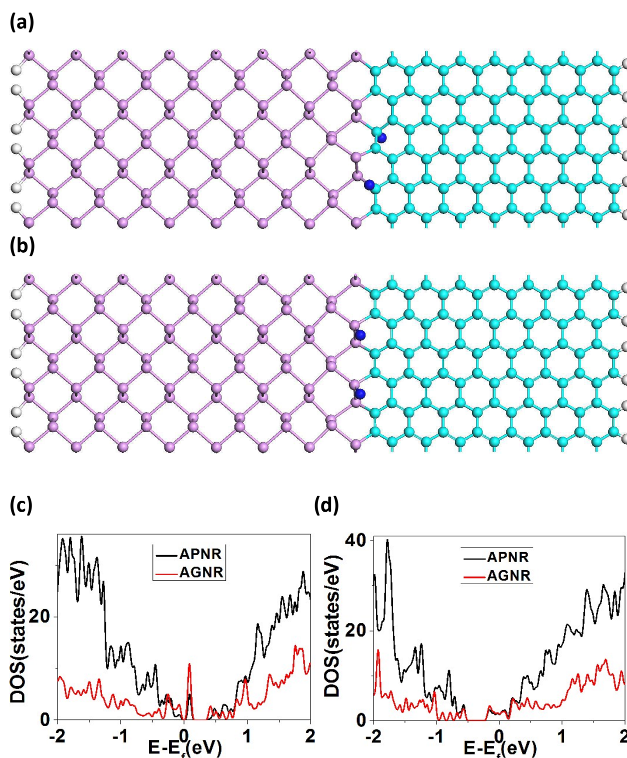

Fig. 4. Optimised structures of (a) configuration 1 and (b) configuration 2. DOS of (c) configuration 1 and (d) configuration 2. H adatoms are blue.

Physical Chemistry Chemical Physics Accepted Manuscript

Please do not adjust margins

3.4 Thickness dependent electronic properties

For both phosphorene and graphene, the interlayer coupling can strongly influence the electronic properties. The weak van der Waals interactions between layers can reduce the band gap of multilayered phosphorene and increase the carriers' effective masses of multilayered graphene. This indicates the significance of the study of the multilayered heterostructures of APNRs/AGNRs. For all of the multilayered heterostructures of APNRs/AGNRs investigated, the stacking of APNRs persists in the order of bulk phosphorene. Hexagonal BN is a good insulator and dielectric material. The lattices of hexagonal BN match well with phosphorene along the armchair direction. We investigate the heterostructures of APNRs/armchair BN nanoribbons (ABNNRs) for a comparison. The relaxed structure of monolayer 15-APNR/15-ABNNR is shown in Figs. 5(a) and 5(b). As shown in Fig. 5(c), this heterostructure has a direct band gap of 0.72 eV. The states near Fermi level are all contributed from 15-APNR (see 5(d)). 15-ABNNR has a band gap of 1.81 eV.

The relaxed structures of quadlayer 15-APNR/15-AGNR and 15-APNR/15-ABNNR are shown in Figs. 6(a) and 6(b), respectively. The relaxed structures of these two heterostructures are similar. There exists strong structural deformation at the interface, especially on the graphene and BN parts. The thickness-dependent band gaps of the heterostructures of APNRs/AGNRs and APNRs/ABNNRs are shown in Tables I and II, respectively. For the heterostructures of APNRs/AGNRs and APNRs/ABNNRs, the band gaps decrease rapidly as the thickness is increased. The band structures of quadlayer 15-APNR/15-AGNR and 15-APNR/15-ABNNR are shown in Figs. 6(c) and 6(d), respectively. Their band gap sizes are zero and 0.24 eV, respectively. Although the thickness is increased, the multilayered heterostructures of APNRs/AGNRs and APNRs/ABNNRs persist in the characteristics of the direct band gap. In addition, the transport properties are thickness dependent. The effective masses of the hole carriers for monolayer, bilayer, trilayer and quadlayer 15-APNR/15-AGNR are 0.18, 0.23, 0.26 and 0.28 m_0, respectively. The effective masses of electron carriers for monolayer, bilayer, trilayer and quadlayer 15-APNR/15-AGNR are 0.18, 0.20, 0.21 and 0.23 m_0, respectively. Thus, the thicker the heterostructures of APNRs/AGNRs, the larger the effective masses of the carriers. Similar effects were also found in the heterostructures of 15-APNR/15-ABNNR. The effective masses of the hole carriers for monolayer, bilayer, trilayer and quadlayer 15-APNR/15- ABNNR are 0.19, 0.22, 0.25 and 0.27 m_0, respectively. The effective masses of the electron carriers for monolayer, bilayer, trilayer and quadlayer 15-APNR/15- ABNNR are 0.22, 0.27, 0.30 and 0.31 m_0, respectively.

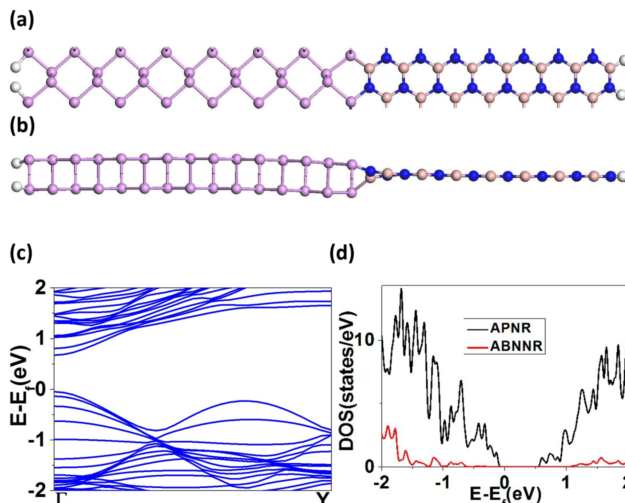

Fig. 5. (a) Top and (b) side views of the relaxed heterostructure of monolayer 15-APNR/15-ABNNR. (c) Band structure and (d) DOS of monolayer 15-APNR/15-ABNNR.

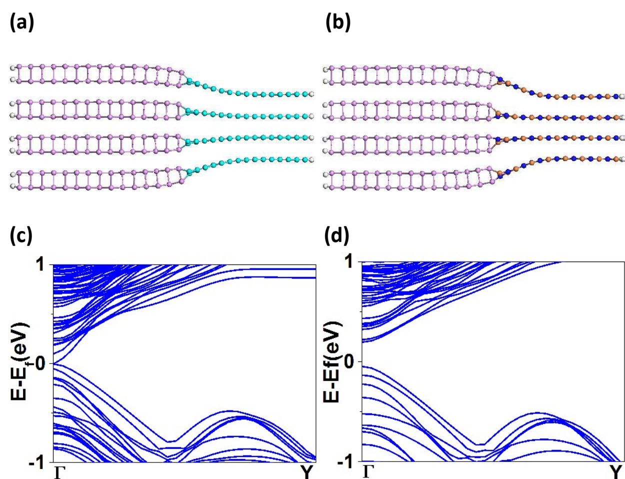

Fig. 6. Relaxed structures of quadlayer (a) 15-APNR/15-AGNR and (b) 15-APNR/15-ABNNR. Band structures of quadlayer (c) 15-APNR/15-AGNR and (d) 15-APNR/15-ABNNR.

Table 1 Band gaps (eV) of five heterostructures of APNRs/AGNRs versus the thickness.

	Monolayer	Bilayer	Trilayer	Quadlayer
16-APNR/16-AGNR	0.65	0.06	0.03	0
15-APNR/16-AGNR	0.66	0.07	0.05	0.02

Physical Chemistry Chemical Physics Accepted Manuscript

 This journal is © The Royal Society of Chemistry 20xx

Please do not adjust margins

15-APNR/15-AGNR	0.45	0.05	0.03	0
12-APNR/12-AGNR	0.53	0.17	0.04	0.01
9-APNR/9-AGNR	0.61	0.28	0.18	0.09

Table 2 Band gaps (eV) of five heterostructures of APNRs/ABNNRs versus the thickness.

	Monolayer	Bilayer	Trilayer	Quadlayer
16-APNR/16-ABNNR	0.69	0.38	0.31	0.23
15-APNR/16-ABNNR	0.70	0.38	0.31	0.24
15-APNR/15-ABNNR	0.72	0.39	0.30	0.24
12-APNR/12-ABNNR	0.74	0.40	0.32	0.25
9-APNR/9-ABNNR	0.82	0.50	0.38	0.28

3.4 Transport properties of two-probe devices

The transport properties of two-probe devices of graphene/phosphorene/graphene along the zigzag directions are investigated. A two-probe device is shown in Fig. 7(a). Four devices with scattering regions that contain 3, 7, 11 and 15 atomic P layers are investigated. The transmission coefficients of these four devices at zero bias are shown in Fig. 7(b). Except the device with 3 P layers, all of the devices exhibit semiconducting transport characteristics. The device with 3P layers has a tiny transport gap and exhibits semimetal transport properties. Near Fermi level, the device with 3 P layers has the largest transmission coefficient. The transmission coefficients around Fermi level are attenuated as the thickness of the phosphorene is increased. According to the Landauer formula, the conductance of the device is defined by $G=G_0T(E_f)$, where $T(E_f)$ is the transmission coefficient of the Fermi level and $G_0=2e^2/h$ is the quantum transport unit. From Fig. 7(b), the transmission coefficients of the Fermi level of the four devices with scattering regions containing 3, 7, 11 and 15 atomic P layers are 1.3×10^{-4}, 3.5×10^{-5}, 8.0×10^{-6} and 1.8×10^{-6}, respectively. Thus, the corresponding conductances are 1.3×10^{-4}, 3.5×10^{-5}, 8.0×10^{-6} and 1.8×10^{-6} G_0, respectively. As expected for the tunnelling transport, the results exhibited an exponential decay of G with $G= G_c e^{-\beta N}$, where G_c is the pre-exponential factor, N is the number of P layers and β is the exponential decay factor.[40] The transmission coefficient decays as $e^{-\beta}$ if the thickness of the phosphorene is increased by one layer. Here, we can extract a β of 0.36. The calculated current-voltage (*I-V*) characteristics are shown in Fig. 7(c). The charge current is calculated from the Landauer–Büttiker formula

$$I=\frac{2e}{h}\int_{\mu_L}^{\mu_R} dE\,T(E,V_b)[f(E-\mu_L)-f(E-\mu_R)] \quad (5)$$

where μ_L/μ_R are the electrochemical potentials of the left and right electron reservoirs, respectively; f is the Fermi–Dirac distribution function of the electron reservoirs; $V_b=\mu_L-\mu_R/e$ is the voltage bias applied to the devices; and $T(E,V_b)$ is the bias dependent transmission coefficient. The device with 3 P layers needs the smallest bias to open the transport gap. A larger bias of 0.95 V is needed for the device with 15 P layers to be conductive. Similarly, a 1.15 eV transport gap of monolayer phosphorene devices with gold electrodes was found.[8] This proves the capability of graphene as electrodes can be comparable to gold, which mainly relies on the delocalised 5s electrons. The wider the phosphorene scattering region, the larger the transport gap. One feasible way to reduce the transport gap and further tune the transport properties is to add the gate bias, which can be realized in the experiments. The proposed two-probe device with graphene electrodes is different from the traditional two-probe devices with metals as the electrodes. Using graphene as an electrode reduces the size of the devices based on phosphorene. Graphene is also a naturally better electrode for phosphorene compared to metals due to its tiny lattice mismatch. This can solve the fundamental contact problem for the application of phosphorene in electronic devices.

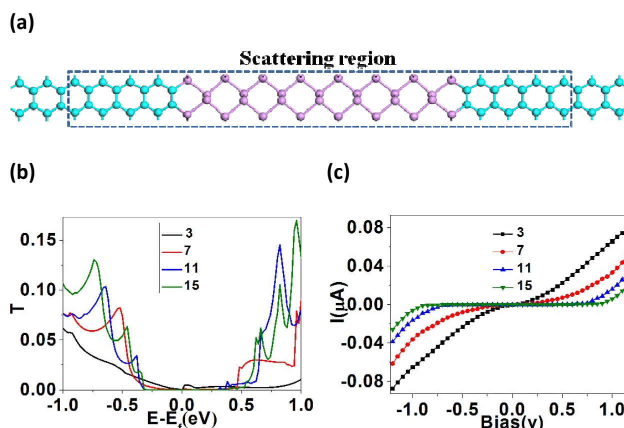

Fig. 7. (a) Structure of the two-probe device of graphene/phosphorene/graphene with 15 atomic layers P. (b) Transmission coefficients of the four two-probe devices at zero bias. (c) I-V curves of the four devices.

Physical Chemistry Chemical Physics Accepted Manuscript

This journal is © The Royal Society of Chemistry 20xx

Please do not adjust margins

The energy band diagram of contact between monolayer graphene and phosphorene is shown in Fig. 8. The work function (W_m) of graphene monolayer is 4.6 eV. Because there is lack of experimental measurements of the work function of monolayer phosphorene, we use the calculated value of 5.1 eV, which is in good agreement with other theoretical calculations.[41, 42] Because graphene is a semimetal and its work function is smaller than that of phosphorene, the electrons will flow to phosphorene. This leads to band bending down of the phosphorene at the interface. Correspondingly, there is an energy barrier at the interface, which will block the graphene electrons from entering the phosphorene. The Schottky barrier for the electron flow is

$$e\phi_{Bn} = W_m - \chi \quad (6)$$

where χ is the electron affinity of the monolayer phosphorene. For the pristine monolayer phosphorene, the band gap E_g and W_m are 2.0 and 5.1 eV, respectively, thus we can get an χ of 4.1 eV. Thus, $e\phi_{Bn}$ is 0.5 eV. The Schottky barrier for the hole flowing from phosphorene to graphene is

$$e\phi_{Bp} = E_g - e\phi_{Bn} \quad (7)$$

Here, we can get an $e\phi_{Bp}$ of 1.5 eV.

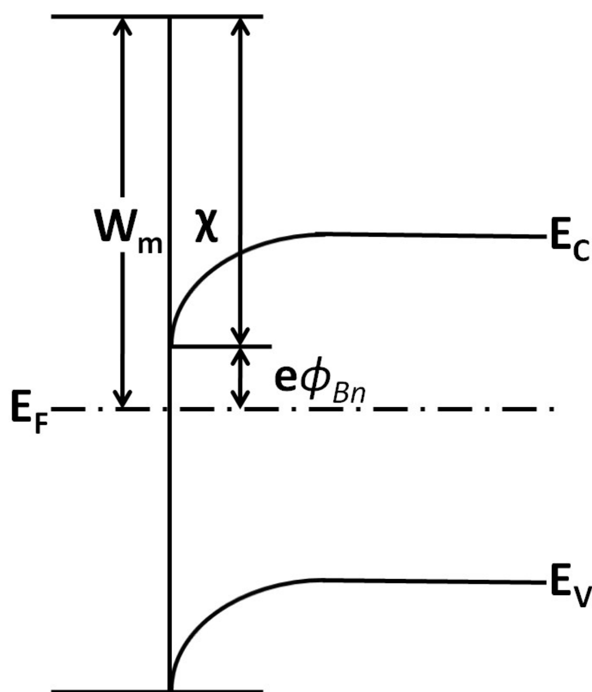

Fig. 8. Scheme of the energy band alignment diagram of the contact between monolayer graphene and phosphorene.

IV. Conclusions

In summary, the band gaps, carriers' effective masses and work functions of the heterostructures of phosphorene/graphene can be modulated by the quantum size effects. A tranverse E_{ext} can effectively reduce the band gaps of the heterostructures and even result in semiconductor-to-metal transition. H doping can tune these heterostructures into either metals or magnetic semiconductors. The band gaps and carriers' effective masses of multilayered heterostructures are dependent on the thickness. Graphene is a naturally better electrode for phosphorene compared to metals due to its tiny lattice mismatch. The transport properties of two-probe devices of graphene/phosphorene/graphene exhibit tunnelling transport characteristics. It is expected that some of the physical properties predicted here can be measured by STM, infrared spectroscopy and scanning Kelvin probe. The interface of phosphorene/graphene also demonstrates the possibility to fabricate a new type of heterostructure by rectangular and hexagonal lattices and that the advantages of these two different types of two-dimensional material can be integrated in one layer.

[a] *College of Physics and Technology and Shenzhen Key Laboratory of Sensor Technology, Shenzhen University, Shenzhen 518060, Guangdong, P. R. China. E-mail: duyu@szu.edu.cn*
[b] *Department of Electronic Engineering and Materials Science and Technology Research Center, The Chinese University of Hong Kong, Shatin, N.T., Hong Kong SAR, People's Republic of China E-mail: jbxu@ee.cuhk.edu.hk*
[c] *Department of Mechanical Engineering and Materials Science, Department of Chemistry, and the Smalley Institute for Nanoscale Science and technology, Rice University, Houston, Texas 77005, USA. E-mail: biy@rice.edu*
† Footnotes relating to the title and/or authors should appear here.
Electronic Supplementary Information (ESI) available: [details of any supplementary information available should be included here]. See DOI: 10.1039/x0xx00000x

Acknowledgements

The authors gratefully acknowledge the financial support from NSFC (No. 11304206 and No. 11375117), Strategic Emerging Industry Development Special Fund of Shenzhen (JCYJ20140418095735562 and JCYJ20130326111743703), and NSFSZU (No. 827000001).

Physical Chemistry Chemical Physics Accepted Manuscript

This journal is © The Royal Society of Chemistry 20xx

Notes and reference

[1] L. K. Li, Y. J. Yu, G. J. Ye, Q. Q. Ge, X. D. Ou, H. Wu, D. L. Feng, X. H. Chen and Y. B. Zhang, *Nat. Nanotech.* , 2014, 9, 372-377.

[2] S. Das , W. Zhang , M. Demarteau, A. Hoffmann, M. D. Dubey, and A. Roelofs, *Nano Lett.* , 2014, 14, 5733-5739.

[3] L. B. Liang , J. Wang , W. Z. Lin , B. G. Sumpter , V. Meunier , and M. Pan, *Nano Lett.* , 2014, 14 , 6400-6406.

[4] G. X. Wang, R. Pandey and S. P. Karnab, *Nanoscale*, 2015, 7, 524-531

[5] J. Dai and X. C. Zeng, *J. Phys. Chem. Lett.*, 2014, 5, 1289-1293.

[6] T.-H. Liua and C.-C. Chang, *Nanoscale*, 2015, 7, 10648-106544

[7] L. Q. Wang, A. Kutana, X. L. Zou and B. I. Yakobson, *Nanoscale*, 2015, 7, 9746-9751

[8] Y. H. Xu, J. Dai, and X. C. Zeng, *J. Phys. Chem. Lett.* 2015, 6, 1996–2002

[9] F. Schwierz, J. Pezoldt and R. Granzner, *Nanoscale*, 2015, 7, 8261-8283

[10] J. S. Qiao, X. H. Kong, Z.-X. Hu, F. Yang, and W. Ji, *Nat. Commun.* 2014, 5, 4475

[11] G. Z. Qin, Q. B. Yan, Z. Z. Qin, S.-Y. Yue, M. Hu and G. Su, *Phys. Chem. Chem. Phys.*, 2015, 17, 4854-4858

[12] X. Y. Han, H. M. Stewart, S. A. Shevlin, C. R. A. Catlow, and Z. X. Guo, *Nano Lett.*, 2014, 14, 4607-4614

[13] A. S. Rodin, A. Carvalho, and A. H. Castro Neto, *Phys. Rev. Lett.*, 2014, 112, 176801

[14] X. L. Sui, C. Si, B. Shao, X. L. Zou, J. Wu, B.-L. Gu, and W. H. Duan, *J. Phys. Chem. C*, 2015, 119, 10059–10063

[15] W. Y. Yu, Z. L. Zhu, C. Y. Niu, C. Li, J.-H. Cho, and Y. Jia, *Phys. Chem. Chem. Phys.*, 2015, 17, 16351-16358.

[15] D. W. Boukhvalov, A. N. Rudenko, A. Prishchenko, V. G. Mazurenkoc and M. I. Katsnelson, *Phys.Chem.Chem.Phys.*,2015, 17, 15209-15217.

[16] L. Seixas, A. Carvalho, and A. H. Castro Neto, *Phys. Rev. B.*,2015, 91, 155138.

[17] G.-C. Guo, X.-L.Wei, D. Wang, Y. P. Luo, and L.-M. Liu, *J. Mater. Chem. A*, 2015, 3,11246

[18] A. Hashmi, and J. Hong, *J. Phys. Chem. C*, 2015, 119, 9198–9204

[19] Y. Jing, Q. Tang, P. He, Z. Zhou and P. W. Shen, *Nanotechnology*, 2015, 26, 095201

[20] X. Q. Tian, L. Liu, Y. Du, J. Gu, J.-B. Xu and B. I. Yakobson, *Phys. Chem. Chem. Phys.*, 2015, 17, 1831-1836.

[21] P. Sutter, R. Cortes, J. Lahiri, and E. Sutter, *Nano Lett.*, 2012, 12, 4869-4874.

[22] X.Q. Tian, Y. D. Wei, S. A. Edwards, Y. J. Yu, X. M. Cai, J.-B. Xu, *Appl. Surf. Sci.*, 2014, 292 237–246.

[23] J. Sun, G. Y. Zheng, H.-W. Lee, N. Liu, H. T. Wang, H. B. Yao, W. S. Yang, and Y. Cui, *Nano Lett.*, 2014, 14 , 4573-4580.

[24] P. Giannozzi, et al., *J. Phys.: Condens. Matter*, 2009, 21, 395502.

[25] P. E. Blöchl, *Phys. Rev. B*, 1994, 50, 17953–17978.

[26] J. P. Perdew, K. Burke and M. Ernzerhof, *Phys. Rev. Lett.*,1996, 77, 3865.

[27] S. Grimme, *J. Comp. Chem.*, 2006, 27, 1787-1799.

[28] J. Taylor, H. Guo, J. Wang, *Phys. Rev. B*, 2001, 63, 245407.

[29] R. Gholizadeh and Y.-X. Yu, *J. Phys. Chem. C*, 2014, 118, 28274-28282.

[30] G. Giovannetti, P. A. Khomyakov, G. Brocks, V. M. Karpan, J. van den Brink, and P. J. Kelly, *Phys. Rev. Lett.*, 2008, 101, 026803.

[31] Y.-J. Yu, Y. Zhao, S. Ryu, L. E. Brus, K. S. Kim, and P. Kim, *Nano Lett.*, 2009, 9, 3430-3434.

[32] K. Dolui, C. Das Pemmaraju and S. Sanvito, *ACS Nano*,2012, 6, 4823-4834.

[33] V. Tran and L.Yang, *Phys. Rev. B.*,2014, 89, 245407.

[34] Y.-W. Son, Marvin L. Cohen, and S. G. Louie, *Phys. Rev. Lett.*, 2006, 97, 216803.

[35] K. F. Mak, C. H. Lui, J. Shan, T. F. Heinz, *Phys. Rev. Lett.* 2009, 102, 56405.

[36] J. E. Johns, M. C. Hersam, *Acc. Chem. Res.*, 2013, 46, 77-86.

[37] X. Q. Tian, J. B. Xu, and X. M. Wang *J. Phys. Chem. B*, 2010, 114, 11377–11381

[38] X. Q. Tian, J. Gu, and J. B. Xu, *J. Chem. Phys.*, 2014, 140, 044712

[39] A. K. Singh, B. I. Yakobson, *Nano Lett.*, 2009, 9, 1540-1543

[40] E. Prodan, and R. Car, *Nano Lett.*, 2008, 8, 1771-1777.

[41] K. Gong, L. Zhang, W. Ji, and H. Guo, *Phys. Rev. B.*,2014, 90, 125441.

[42] Y. Q. Cai, G. Zhang, and Y.-W. Zhang, *Sci. Rep.*,2014, 4, 6677.

Physical Chemistry Chemical Physics Accepted Manuscript

Physical Chemistry Chemical Physics Accepted Manuscript

TOC graphic

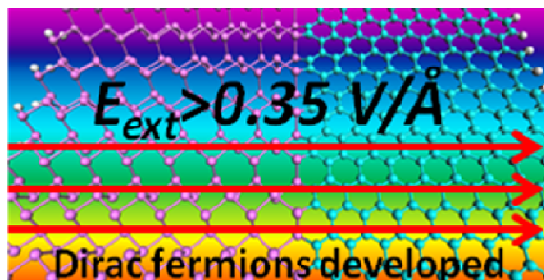

This journal is © The Royal Society of Chemistry 20xx